J. Fluid Mech. (1989), *vol.* 201, *pp.* 167–188
Printed in Great Britain

On the motion of a gas experiencing range-dependent volumetric heating

By J. R. TORCZYNSKI
Fluid and Thermal Sciences Department, Sandia National Laboratories, Albuquerque, NM 87185, USA

(Received 19 February 1988 and in revised form 18 August 1988)

The motion of a perfect gas in a closed geometry is studied when it experiences large, transient, spatially non-uniform volumetric heating caused by the passage of energetic particles or intense light through the gas. The spatial non-uniformity of the heating results from the fact that the energy deposition in the gas is characterized by a range, a lengthscale which is inversely proportional to the local gas density. The equations of motion of the gas are acoustically filtered and then specialized to a one-dimensional problem. When written in Lagrangian form, the equations are reduced to a system of ordinary differential equations. Because of the special form of the one-dimensional range-dependent volumetric heating source term, this system can be solved analytically. Limitations on the applicability of this approximate analytical solution are discussed. Numerical simulations of specific cases for which the solution is valid are in agreement with the solution.

1. Introduction

The passage of energetic particles or intense light through a sample of gas results in a volumetric energy deposition within the gas. This energy deposition is largest near the origin of the particles or photons and small (possibly zero) when the distance from the origin to the observation point within the gas exceeds the *range*, denoted l, essentially the thickness of a gas layer (of specified density) that will absorb most or all of the incident energy flux. This spatial non-uniformity sets up pressure gradients in the gas. As the gas responds to these gradients and flows away from the regions of largest energy deposition, the changing gas density modifies the energy source term. This feedback results from two facts. First, the range in the gas is not a global constant; rather, it is a local quantity inversely proportional to the gas density. Second, the energy deposition depends on the range, and hence the gas density, in a non-local fashion: the energy flux at a certain location in the gas depends on the integral $\int l^{-1}\,\mathrm{d}s$, which is proportional to $\int \rho\,\mathrm{d}s$, along the path from the particle or photon origin to the observation point. The power density source term is given by the negative of the divergence of this flux and as such is a function of the integral $\int \rho\,\mathrm{d}s$ and also is proportional to the gas density at the observation point.

Problems of this sort occur in many different contexts. Absorption of infrared light by gas mixtures containing carbon dioxide or other polyatomic species can be described by the above model under certain circumstances (Plass & Yates 1965). One example involving particles is the energy deposition from an electron beam propagating through air or other gases (Samlin & Patterson 1987). Another important example involves the passage of fission fragments through a gas. Typically, thermal neutrons are employed to induce nuclear reactions in a thin layer

of fissile material coating the inner surface of a gas-filled container (Miley 1970). Some of the fission fragments thus produced escape into the gas and deposit energy there, a process referred to henceforth as pumping. The fission-fragment energy source term depends on the fission-fragment ranges in the gas and therefore affects the gas density field as described above.

Applications of fission-fragment energy deposition involve direct conversion of nuclear energy into electricity (Miley 1970) or coherent light (Miley 1970; McArthur & Tollefsrud 1975). In devices such as electrical cells and nuclear-reactor-pumped lasers, it is important to know the spatial and temporal variation of the energy source term within the gas. This requires an understanding of the gas motion and resultant density changes. Furthermore, knowledge of the density field inside a nuclear-reactor-pumped laser cavity is essential for calculations of optical mode shapes and beam steering within the laser cavity. This is because the index of refraction is equal to unity plus a term proportional to the gas density (Born & Wolf 1980, pp. 87–90).

Some numerical calculations have been performed recently to analyse the gasdynamics of electron-beam pumping (Samlin & Patterson 1987) and fission-fragment pumping (Torczynski & Gross 1986; Neal *et al.* 1987). Although useful to model individual experiments, these simulations provide little physical insight. Moreover, prediction of trends is laborious, requiring simulation of many different cases. Also, in the works mentioned above, other sources of spatial variation were included in the pumping, and the resulting additional complexity of the gas motion often obscured the role of the range dependence. Thus, an analytical approach is desirable to isolate and elucidate the interaction of the range-dependent energy source term with the gasdynamics.

2. The acoustically filtered equations of motion

Consider a perfect, inviscid, non-conducting gas which is initially in a motionless, uniform thermodynamic state (pressure p_0, temperature T_0, and density ρ_0). It is confined within a closed volume V with surface S, through which an energy flux carried by particles or photons is introduced. The energy is absorbed within the gas although some of the particles or photons may completely traverse the chamber and be lost. The volumetric heating thus produced is denoted by Q. A detailed description of this term for the special case of fission-fragment heating is given in Appendix A.

The equations describing the motion of the gas are the conservation equations for mass, momentum, and energy

$$\frac{\partial}{\partial t}\rho + \boldsymbol{\nabla}\cdot\rho\boldsymbol{u} = 0, \tag{2.1}$$

$$\frac{\partial}{\partial t}\rho\boldsymbol{u} + \boldsymbol{\nabla}\cdot\rho\boldsymbol{u}\boldsymbol{u} = -\boldsymbol{\nabla}p, \tag{2.2}$$

$$\frac{\partial}{\partial t}\rho(e+\tfrac{1}{2}u^2) + \boldsymbol{\nabla}\cdot\rho\boldsymbol{u}(e+p/\rho+\tfrac{1}{2}u^2) = Q, \tag{2.3}$$

and the equation of state for a perfect gas

$$p = R\rho T = (\gamma-1)\rho e. \tag{2.4}$$

A suitable combination of the above four equations yields

$$\frac{\partial p}{\partial t}+\gamma p\nabla\cdot\boldsymbol{u}+\boldsymbol{u}\cdot\nabla p=(\gamma-1)\,Q. \tag{2.5}$$

Note that the coupling of the heat addition and the gas motion vanishes as γ approaches unity because in this limit a gas molecule stores energy in its many internal degrees of freedom, rather than in its three translational degrees of freedom (pressure).

At this point, acoustic filtering can be applied to the above equations. As discussed by Rehm & Baum (1978), Paolucci (1982), Baum *et al.* (1983), and Schutt & Baer (1987), the acoustic-filtering methodology acts to remove sound waves from the equations of motion. In the context of the heat-addition problems considered here, the heat addition must be slow (this will be quantified below – see also the above references) so that the acoustic pressure perturbations produced by the spatial non-uniformity of the heating are small compared with the mean pressure. Thus, acoustic filtering involves making the assumption that the spatial variations of the pressure, denoted $\hat{p}$, are small compared with the mean pressure, denoted $\bar{p}$ (the latter is a function of time alone). In some sense, it seems paradoxical to make such an assumption since the pressure gradients drive the motion; however, the justification for this assumption is that the Mach numbers of the flow are much smaller than unity (see Appendix B) and hence the pressure variations within V are small compared with the mean pressure. Limitations on the theory imposed by this assumption are discussed in a later section. The acoustically filtered version of (2.5) is

$$\frac{\mathrm{d}\bar{p}}{\mathrm{d}t}+\gamma\bar{p}\nabla\cdot\boldsymbol{u}=(\gamma-1)\,Q. \tag{2.6}$$

Equation (2.6) can be partitioned into two equations in the following manner. Integrate (2.6) over the volume V and normalize the result by V. The resulting equation,

$$\frac{\mathrm{d}\bar{p}}{\mathrm{d}t}=(\gamma-1)\,\bar{Q}(t), \tag{2.7}$$

describes the time evolution of the pressure in terms of $\bar{Q}$, the spatial average of the energy source term, where

$$\bar{Q}(t)\equiv\frac{1}{V}\int_V Q(t,\boldsymbol{x})\,\mathrm{d}^3\boldsymbol{x}. \tag{2.8}$$

Note in passing that the integral over V of the second term in (2.6) is zero since by Gauss' theorem the volume integral can be converted into a surface integral involving the normal component of the velocity, which vanishes identically on the boundary. (In the event that gas could enter or leave the enclosure through an opening in the wall, an additional term, resulting from the mass flow through this opening, would appear in (2.7) by virtue of this surface integral. A relation determining the flow rate in terms of the internal and external pressures would then be necessary (Rehm & Baum 1978). Appendix C contains a brief discussion of the theory in the absence of walls.) Subtracting (2.7) from (2.6) yields a relation for the divergence of the velocity,

$$\gamma\bar{p}\nabla\cdot\boldsymbol{u}=(\gamma-1)\,\hat{Q}(t,\boldsymbol{x}), \tag{2.9}$$

in terms of $\hat{Q}$, the difference between the source term and its spatial average, where

$$\hat{Q}(t,\boldsymbol{x})\equiv Q(t,\boldsymbol{x})-\bar{Q}(t). \tag{2.10}$$

The pressure variations cannot be ignored in (2.2); however, the gradient of the mean pressure vanishes identically, leaving

$$\frac{\partial}{\partial t}\rho \boldsymbol{u} + \boldsymbol{\nabla}\cdot\rho\boldsymbol{u}\boldsymbol{u} = -\boldsymbol{\nabla}\hat{p}. \tag{2.11}$$

When combined with an explicit form for the volumetric energy source term Q, (2.1), (2.7), (2.9), and (2.11), together with definitions (2.8) and (2.10) and the normal velocity boundary condition,

$$\boldsymbol{u}\cdot\hat{\boldsymbol{n}} = 0, \tag{2.12}$$

form a closed system of equations describing the motion of a gas experiencing non-uniform volumetric heating.

3. The one-dimensional problem

3.1. *Equations of motion*

Consider the case of a gas confined between two infinite parallel walls separated by a distance $D = 2L$. At some point in time, equal and opposite energy fluxes enter the gas from the two walls. Volumetric absorption of the energy by the gas gives rise to the energy source term Q. The situation described above is one-dimensional and symmetric. The coordinate x is defined such that the wall inner surfaces are located at $x = \pm L$. The centreplane ($x = 0$) is thus the plane of symmetry, so henceforth only the region from $x = 0$ to $x = L$ will be considered. In this region, the motion of the gas is described by the one-dimensional versions of (2.1), (2.7), (2.8), (2.9), and (2.10):

$$\frac{\partial\rho}{\partial t} + u\frac{\partial\rho}{\partial x} + \rho\frac{\partial u}{\partial x} = 0, \tag{3.1}$$

$$\frac{\mathrm{d}\bar{p}}{\mathrm{d}t} = (\gamma-1)\,\bar{Q}, \tag{3.2}$$

$$\gamma\bar{p}\frac{\partial u}{\partial x} = (\gamma-1)\,\hat{Q}, \tag{3.3}$$

$$\bar{Q}(t) \equiv \frac{1}{L}\int_0^L Q(t,x)\,\mathrm{d}x, \tag{3.4}$$

$$\hat{Q}(t,x) \equiv Q(t,x) - \bar{Q}(t). \tag{3.5}$$

Note in passing that it is not necessary to solve (2.11) in a one-dimensional system unless determination of $\hat{p}$ is desired. The boundary conditions for the velocity u are that it must vanish at the centreplane (by symmetry) and at the wall:

$$u(t,0) = u(t,L) = 0. \tag{3.6}$$

3.2 *The range-dependent source term*

In order to form a closed system of equations, a specific representation of the one-dimensional range-dependent volumetric energy source term $Q(t,x)$ at a location x within the gas at time t is required. The source term has the form

$$Q(t,x) = Q_0\,h(t/t_0)f[x;\rho(t,\tilde{x})/\rho_0]. \tag{3.7}$$

Here, Q_0 is the power density scale of the pumping. The function h is a dimensionless

$O(1)$ function giving the time dependence of the pumping pulse, with timescale t_0. It has the properties that $h(-\infty) = 0$ and $h_{\max} = 1$ and frequently has the additional properties that $h(+\infty) = 0$ and that

$$\int_{-\infty}^{+\infty} h(\tau)\,\mathrm{d}\tau$$

is finite (in cases of physical interest, h often resembles a Gaussian function).

The function f, also a dimensionless $O(1)$ function, is determined at a point x by values of the gas density ρ at all points $\tilde{x}$ between 0 and L. Recall that the range l is inversely proportional to the local gas density.

$$l(t,x) = \frac{A_{\mathrm{ref}}}{\rho(t,x)} = l_0\left(\frac{\rho(t,x)}{\rho_0}\right)^{-1}, \tag{3.8}$$

where l_0 has been defined to be

$$l_0 \equiv \frac{A_{\mathrm{ref}}}{\rho_0} \tag{3.9}$$

and A_{ref} is a constant for a given mixture of molecular species. The range-dependent nature of f is manifested through its dependence on two quantities:

$$\int_x^L \frac{\mathrm{d}\tilde{x}}{l(t,\tilde{x})} = \frac{L}{l_0}\left(1 - \frac{1}{L}\int_0^x \frac{\rho(t,\tilde{x})}{\rho_0}\mathrm{d}\tilde{x}\right), \tag{3.10}$$

$$\int_{-L}^x \frac{\mathrm{d}\tilde{x}}{l(t,\tilde{x})} = \frac{L}{l_0}\left(1 + \frac{1}{L}\int_0^x \frac{\rho(t,\tilde{x})}{\rho_0}\mathrm{d}\tilde{x}\right). \tag{3.11}$$

(The equalities result from the symmetry of the problem and from the fact that

$$\int_0^L \rho(t,x)\,\mathrm{d}x = \rho_0 L \tag{3.12}$$

by conservation of mass.) The quantities in (3.10) and (3.11) determine the contributions to f from the energy fluxes entering the chamber at $x = L$ and $x = -L$, respectively. Now the volumetric energy source term is just the negative of the divergence of the particle or photon energy flux, so the function f has the special form

$$f[x;\rho(t,\tilde{x})/\rho_0] = L\frac{\partial}{\partial x}F\left(\frac{1}{L}\int_0^x \frac{\rho(t,\tilde{x})}{\rho_0}\mathrm{d}\tilde{x}\right) = \frac{\rho(t,x)}{\rho_0}F'\left(\frac{1}{L}\int_0^x \frac{\rho(t,\tilde{x})}{\rho_0}\mathrm{d}\tilde{x}\right). \tag{3.13}$$

Here, the derivative of F with respect to its argument is denoted by F'. Without loss of generality, $F(0)$ is taken to be zero. Note that the argument of F and F' is the amount of mass contained between the centreplane ($x = 0$) and the x-location, normalized by the amount of mass contained between the centreplane and the wall. As such, it vanishes at $x = 0$ and rises to unity at $x = L$. Thus, the value of $f[x;\rho(t,\tilde{x})/\rho_0]$ at a point x depends in a non-local fashion on the density field $\rho(t,\tilde{x})$.

The function $F'(\xi)$ has one of two possible forms (see figure 1). In most cases, the function $F'(\xi)$ is positive with positive slope (except at $\xi = 0$, where the slope vanishes by symmetry) and positive concavity. In other cases, however, there may be a value ξ_0 such that $F'(\xi)$ is identically zero in the region $0 \leqslant \xi \leqslant \xi_0$. In the region $\xi_0 < \xi \leqslant 1$, $F'(\xi)$ is positive with positive slope and concavity. In either case, $F'(\xi)$ is smallest (possibly zero) at the centreplane and largest at the walls.

The functions F and F' also have the dimensionless parameter $L/l_0 = \rho_0 L/A_{\mathrm{ref}}$ as

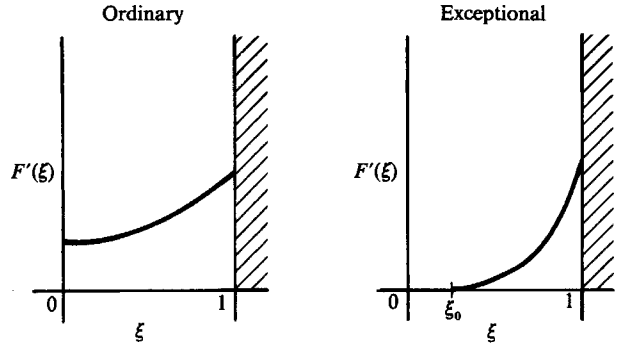

FIGURE 1. The ordinary and exceptional forms of the function $F'(\xi)$.

an argument. Typically, L/l_0 is $O(1)$. If L/l_0 were very small, then only a small fraction of the available energy would be absorbed by the gas. On the other hand, if L/l_0 were very large, then a large portion of the gas would remain essentially unpumped. This and other model-specific dimensionless parameters are important since they determine the specific details of the shape and amplitude of F and F'; however, they are all constant for a given case and therefore will not be listed as additional arguments of F and F'. A detailed account of F and F' and their dimensionless parameters for the special case of fission-fragment energy deposition is given in Appendix A.

3.3. *Special properties of the source term*

The function f, as described by (3.13), has several special properties which make analytical solution of the equations possible. Note that all of the complicated density dependence of f is contained in its argument. Consequently, the computationally intensive multidimensional integral involving ρ which defines f (see Appendix A for the specific case fission-fragment energy deposition) need be calculated for only one density field to determine the functions F and F'. It is convenient to perform these calculations assuming $\rho(t,\tilde{x})/\rho_0 \equiv 1$. In this case, the function F' is seen from (3.13) to be

$$F'(x/L) = L\frac{\partial}{\partial x}F(x/L) = f[x;1]. \tag{3.14}$$

To reiterate, only the argument of F, not the function F itself, varies in time, a fact that will prove to be important.

Another important fact is that the spatial average of $f[x;\rho(t,\tilde{x})/\rho_0]$ is independent of time. Using (3.12) and (3.13), the spatial average of f can be calculated explicitly to be

$$\frac{1}{L}\int_0^L f\,\mathrm{d}x = F(1). \tag{3.15}$$

Note in passing that $F(1)$ is a function of $L/l_0 = \rho_0 L/A_{\mathrm{ref}}$. Since the spatial average of f is constant, it can be used to normalize f and F. Define the normalized functions g and G to be

$$g \equiv f/F(1), \tag{3.16}$$

$$G \equiv F/F(1). \tag{3.17}$$

Now Q, $\bar{Q}$, and $\tilde{Q}$ can be re-expressed using g and G:

$$Q(t,x) = \bar{Q}g, \tag{3.18}$$

$$\bar{Q}(t) = Q_0 F(1)\, h(t/t_0), \tag{3.19}$$

$$\tilde{Q}(t,x) = \bar{Q}g - \bar{Q} = \bar{Q}(g-1), \tag{3.20}$$

At this point, an important observation can be made about the form of the function g. Let $x_p(t,x_0)$ be the particle path such that $x_p(-\infty,x_0) = x_0$, where again the coordinate system origin is located at the centreplane. From (3.13), (3.16), and (3.17), evaluation of g at $x = x_p(t,x_0)$ yields the relation

$$g = \frac{\rho(t,x_p(t,x_0))}{\rho_0} G'(x_0/L). \tag{3.21}$$

This follows from the fact that, since $x_p(t,x_0)$ is a particle path, conservation of mass implies that (3.12) can be generalized to

$$\int_0^{x_p(t,x_0)} \rho(t,x)\,\mathrm{d}x = \rho_0 x_0. \tag{3.22}$$

Hence, the source term *following a fluid particle* depends only on the particle's density, its initial position, and the average source term,

$$Q(t,x_p(t,x_0)) = \bar{Q}(t)\, G'(x_0/L) \frac{\rho(t,x_p(t,x_0))}{\rho_0}. \tag{3.23}$$

4. Analytical solution

The original system of three coupled partial differential equations can now be reduced to three uncoupled ordinary differential equations, and this new system of equations can be solved analytically.

First, (3.2) and (3.19) are combined to obtain an equation for the time evolution of the pressure,

$$\frac{\mathrm{d}\bar{p}}{\mathrm{d}t} = (\gamma-1)\, Q_0 F(1)\, h(t/t_0). \tag{4.1}$$

The integration of this equation is straightforward, yielding

$$\frac{\bar{p}(t)}{p_0} = 1 + \frac{(\gamma-1)\, Q_0 F(1)\, t_0}{p_0} H(t/t_0), \tag{4.2}$$

where the function H is defined to be

$$H(\tau) \equiv \int_{-\infty}^{\tau} h(\tilde{\tau})\,\mathrm{d}\tilde{\tau}. \tag{4.3}$$

Next, an equation describing the time evolution of the density of a particle originating at x_0, denoted

$$\rho_p(t,x_0) \equiv \rho(t,x_p(t,x_0)), \tag{4.4}$$

is obtained by combining (3.1), (3.2), (3.3), (3.20), and (3.21) to produce

$$-\frac{1}{\rho_p}\left(\frac{\partial \rho_p}{\partial t}\right)_{x_0} = \frac{1}{\gamma \bar{p}} \frac{\mathrm{d}\bar{p}}{\mathrm{d}t}\left(G'(x_0/L)\frac{\rho_p}{\rho_0} - 1\right). \tag{4.5}$$

The integration of this equation is straightforward, yielding

$$\frac{\rho_p(t,x_0)}{\rho_0} = \frac{1}{G'(x_0/L)+(1-G'(x_0/L))\,(\bar{p}(t)/p_0)^{-1/\gamma}}. \tag{4.6}$$

To complete the solution, all that remains is to solve for the particle path $x_p(t,x_0)$. To do this, the conservation-of-mass equation (3.1) is rewritten in Lagrangian form and combined with (4.6) to produce

$$\left(\frac{\partial x_p}{\partial x_0}\right)_t = G'(x_0/L)+(1-G'(x_0/L))\,(\bar{p}(t)/p_0)^{-1/\gamma}. \tag{4.7}$$

The integration of this equation is straightforward, yielding

$$x_p(t,x_0)/L = G(x_0/L)+(x_0/L-G(x_0/L))\,(\bar{p}(t)/p_0)^{-1/\gamma}. \tag{4.8}$$

Taking the time derivative of (4.8) and using (3.2) yields a relation for the velocity of a particle,

$$u_p(t,x_0) = -\frac{(\gamma-1)\,\bar{Q}(t)\,L(x_p/L-G(x_0/L))}{\gamma\bar{p}(t)}. \tag{4.9}$$

Note that $u \leqslant 0$, with the equality applying only when $h = 0$ or when $x_0 = 0$ or L.

5. Discussion of the solution

5.1. *Implementation*

Summarized below are the main results of the solution: (3.7), (3.19), (3.14), (3.16), (3.17), (4.2), (4.3), (4.8), (4.6), (4.9), and (3.23).

$$Q(t,x) = Q_0\,h(t/t_0)f[x;\rho(t,\tilde{x})/\rho_0] = \bar{Q}(t)\,g[x;\rho(t,\tilde{x})/\rho_0], \tag{5.1}$$

$$\bar{Q}(t) = Q_0\,F(1)\,h(t/t_0), \tag{5.2}$$

$$F'(x/L) = f[x;1], \quad F(0) = 0, \tag{5.3}$$

$$g = f/F(1), \quad G(x/L) = F(x/L)/F(1), \tag{5.4}$$

$$\frac{\bar{p}(t)}{p_0} = 1+\frac{(\gamma-1)\,Q_0\,F(1)\,t_0}{p_0}H(t/t_0), \quad H(\tau) \equiv \int_{-\infty}^{\tau} h(\tilde{\tau})\,\mathrm{d}\tilde{\tau}, \tag{5.5}$$

$$x_p(t,x_0)/L = G(x_0/L)+(x_0/L-G(x_0/L))\,(\bar{p}(t)/p_0)^{-1/\gamma}, \tag{5.6}$$

$$\frac{\rho_p(t,x_0)}{\rho_0} = \frac{1}{G'(x_0/L)+(1-G'(x_0/L))\,(\bar{p}(t)/p_0)^{-1/\gamma}}, \tag{5.7}$$

$$u_p(t,x_0) = -\frac{(\gamma-1)\,\bar{Q}(t)\,L(x_p/L-G(x_0/L))}{\gamma\bar{p}(t)}, \tag{5.8}$$

$$Q_p(t,x_0) = \bar{Q}(t)\,G'(x_0/L)\frac{\rho_p}{\rho_0}. \tag{5.9}$$

Once the shape function $f[x;1]$ is specified (for example, from the detailed model of fission-fragment energy deposition as outlined in Appendix A), the solution is fully determined in terms of this function. Evaluation of the solution can be divided into the following stages:

(i) discretize the system to yield a set of particle initial locations (x_0 values) between 0 and L;

(ii) solve for $F(1)$ and the values of G' and G corresponding to each x_0 value using (5.3) and (5.4) and the explicit model for $f[x;1]$;

(iii) use (5.5) to solve for the pressure at a given time;

(iv) determine the new location of each particle from (5.6), its density from (5.7), its velocity from (5.8), the source term from (5.9), and any other thermodynamic variables from the equation of state.

5.2. *Observations*

Several observations can be made about the results summarized in the above section. The basic structure of the solution represents a smooth flow of gas inward toward the centreplane. Since the quantity $x_0/L - G(x_0/L)$ is positive away from $x_0 = 0$ or L, where it vanishes, all particle velocities are negative, and the particle locations continue to decrease so long as heat is added to the gas. Consider the particle which was originally located at x_m, where $x_0 = x_m$ maximizes the quantity $x_0/L - G(x_0/L)$. By the construction of the function G, there is exactly one such particle, which is hereafter denoted the 'null' particle. From (5.6) and (5.8), it is seen that the null particle has the greatest inward displacement and the largest negative velocity at every time. Moreover, since the quantity $x_0/L - G(x_0/L)$ is maximized at $x_0 = x_m$, the condition $G'(x_m/L) = 1$ is satisfied. Thus, the null particle undergoes no density change as it moves, as shown by (5.7). Actually, this result follows directly from the continuity equation: if $\partial u/\partial x$ vanishes (as it does at the velocity extremum occurring at x_m), then at this point $\mathrm{D}\rho/\mathrm{D}t$ also must vanish. Particles with larger (smaller) x_0 values have values of G' that are correspondingly larger (smaller) than unity and therefore are continually expanded (compressed).

It should be emphasized that all of the phenomena described above are driven by the 'desire' of the source term to become progressively more spatially uniform as time passes. This is made clear by the following physical argument. The initially existing gradients in Q form small pressure gradients (see Appendix B) since the pressure will be very slightly larger or smaller than the mean pressure in regions where Q is larger or smaller than $\bar{Q}$, respectively. Thus, these pressure gradients act to transport gas from regions of large Q to regions of small Q. From (3.23), it is seen that the source term at a point is roughly proportional to the local gas density. A decrease or increase of the gas density in a region of correspondingly large or small Q acts to decrease or increase Q, respectively. Therefore, the gas motion induced by the spatial non-uniformity of Q acts to reduce the spatial non-uniformity of Q. Incidentally, the null particle always receives energy at the average rate, so $Q_p(t, x_m) = \bar{Q}(t)$.

A striking feature of the analytical solution is the fact that the pressure rise is completely decoupled from the details of the gas motion. As it turns out, this is not directly a consequence of the acoustic filtering assumption (which admittedly ignores the very slight variations of pressure that do exist within the gas) but rather follows from the range-dependent form of the energy source term, specifically from the fact that the spatial averages of $f[x;\rho(t,\tilde{x})/\rho_0]$ and hence of $Q(t,x)$ are independent of the details of the density distribution. Thus, the pressure can be calculated at all times of interest without knowledge of the density and/or velocity distributions at these times.

Conversely, the particle positions and densities at a given time depend only on the

known function G and on the value of $\bar{p}(t)/p_0$. The details of the previous history of the pumping, as embodied in the function h, are forgotten except in an integral sense. Thus, the maximum amount of variation that will occur in the density field, and hence in the refractive index field, is determined solely by the maximum pressure rise, which is related by the perfect gas law to the deposited average energy density.

It is instructive to consider what occurs when $\bar{p}(t)/p_0$ becomes large. There are two distinct possibilities. If there is a region $0 \leqslant \xi \leqslant \xi_0$ in which $G'(\xi)$ is identically zero, then the gas density will continue to increase in this region as long as heat addition continues outside this region. Note that the function $G(\xi)$ is also identically zero in this region, so in the region $0 \leqslant x_0 \leqslant L\xi_0$ the relations (5.6), (5.7), and (5.8) simplify considerably:

$$x_p = x_0(\bar{p}/p_0)^{-1/\gamma}, \tag{5.10}$$

$$\rho_p/\rho_0 = (\bar{p}/p_0)^{1/\gamma}, \tag{5.11}$$

$$u_p = -\frac{(\gamma-1)\bar{Q}}{\gamma\bar{p}}x_p. \tag{5.12}$$

Note that the density is compressed uniformly in this region and hence the velocity is strictly linear in distance from the centreplane. The above equations describe isentropic compression of the gas, as must be the case since no heat (entropy) is deposited in this region by the source term (it is quite generally true that $Ds/Dt = RQ/p$).

If $G'(\xi)$ is strictly positive, the following results hold:

$$\frac{x_p}{L} \to G\left(\frac{x_0}{L}\right), \tag{5.13}$$

$$\frac{\rho_p}{\rho_0} \to \frac{1}{G'(x_0/L)}, \tag{5.14}$$

$$u_p \to 0, \tag{5.15}$$

$$Q_p \to 0, \tag{5.16}$$

In this case, a limiting density profile is reached. As implied above, the time required to approach this limiting density profile is the time required for the pressure to greatly exceed the initial pressure. More precisely, this time t_L is given from (5.6) and (5.7) by

$$\left(\frac{\bar{p}(t_L)}{p_0}\right)^{1/\gamma} \gg \max_{0\leqslant\xi\leqslant1}\left\{\frac{|1-G'(\xi)|}{G'(\xi)}, \frac{(\xi-G(\xi))}{G(\xi)}\right\} = \max\left\{\frac{1}{G'(0)}-1, 1-\frac{1}{G'(1)}\right\}. \tag{5.17}$$

It should be observed that the approach to the steady density profile is algebraic in the pressure ratio and as such is usually a 'slow' process (not exponential in time).

Note that dependence of t_L on p_0. Consider two experiments identical in all respects except that the p_0 and T_0 values to be used in the second experiment are the values used in the first experiment reduced by the same factor (the ρ_0 values are thus the same). Now the average energy deposition and hence the pressure *change* depend on the similarity parameter $L/l_0 = \rho_0 L/A_{ref}$ and on Q_0, t_0, and the details of h. These quantities are the same by design for the two experiments, so the pressure change $\bar{p}(t)-p_0$ is also the same. However, $\bar{p}(t)/p_0$ will rise much more rapidly in the second experiment, which has the lower value of p_0, than in the first experiment. Thus, the second experiment has the smaller t_L value and will show larger density variations

sooner than the first experiment. This is usually viewed as undesirable. Nevertheless, if t_L is smaller than t_0 for the second experiment but not for the first experiment, then the density field will vary continually throughout the pulse in the first experiment but will reach a steady state before the pulse has terminated in the second experiment. A quasi-steady situation (continuing energy deposition without further gas motion), such as occurs for $t > t_L$ in the second experiment, is often desirable.

5.3. *Applicability of the theory*

At this point, it is useful to consider limitations on the applicability of this theory. For the concept of acoustic filtering to be meaningful in this problem, the energy deposition must be 'slow' in some sense. A constraint emerges naturally out of this idea – the time for an acoustic wave to travel across the physical domain must be small compared to the timescale t_0, or

$$\frac{L}{c_0 t_0} \ll 1. \tag{5.18}$$

Here, the quantity c_0 is the initial speed of sound in the gas. If this constraint were violated, then considerable energy would be deposited in the gas before pressure equilibrium could be reached.

It is also necessary to constrain the maximum induced velocity to be much smaller than c_0. Otherwise, large pressure gradients, which the theory assumes are not present, would be dynamically built up. Let U_M be the largest velocity produced in the system,

$$U_M = \max_{x_0, t} \{|u(t, x_p(t, x_0))|\}. \tag{5.19}$$

Substituting (5.8) into (5.19) and requiring $U_M \ll c_0$ yields the constraint

$$(U_B/c_0)\{\xi_m - G(\xi_m)\} \max_{-\infty \leqslant \tau \leqslant +\infty} \left\{ \frac{h(\tau)}{\left(1 + \gamma \dfrac{U_B/c_0}{L/c_0 t_0} H(\tau)\right)^{(\gamma+1)/\gamma}} \right\} \ll 1, \tag{5.20}$$

where the velocity scale U_B is defined to be

$$U_B = \frac{(\gamma - 1) L Q_0 F(1)}{\gamma p_0} \tag{5.21}$$

and $\xi_m = x_m/L$ corresponds to the null particle. Note that both of the bracketed quantities in (5.20) are less than unity (the first bracketed quantity may be much less than unity if the gap separating the walls is much smaller than the range in the gas, that is, if $L/l_0 \ll 1$).

Now the constraint given in (5.18) is usually sufficient to guarantee that $U_M/c_0 \ll 1$. If $U_B/c_0 \ll 1$, then (5.20) is trivially satisfied. If U_B/c_0 and H are $O(1)$ or larger, then (5.20) can be expanded to give

$$\frac{U_M}{c_0} \approx \frac{(L/c_0 t_0)^{(\gamma+1)/\gamma}}{(U_B/c_0)^{1/\gamma}} \frac{(\xi_m - G(\xi_m))}{(\gamma H)^{(\gamma+1)/\gamma}} \ll 1, \tag{5.22}$$

which is clearly satisfied by virtue of (5.18). If, however, step, top-hat, or other discontinuous or rapidly varying functions for h are admitted (essentially letting h change arbitrarily fast, so that h can be $O(1)$ while H is still very small), then in addition to (5.18) it would be necessary to require

$$(U_B/c_0)(\xi_m - G(\xi_m)) \ll 1. \tag{5.23}$$

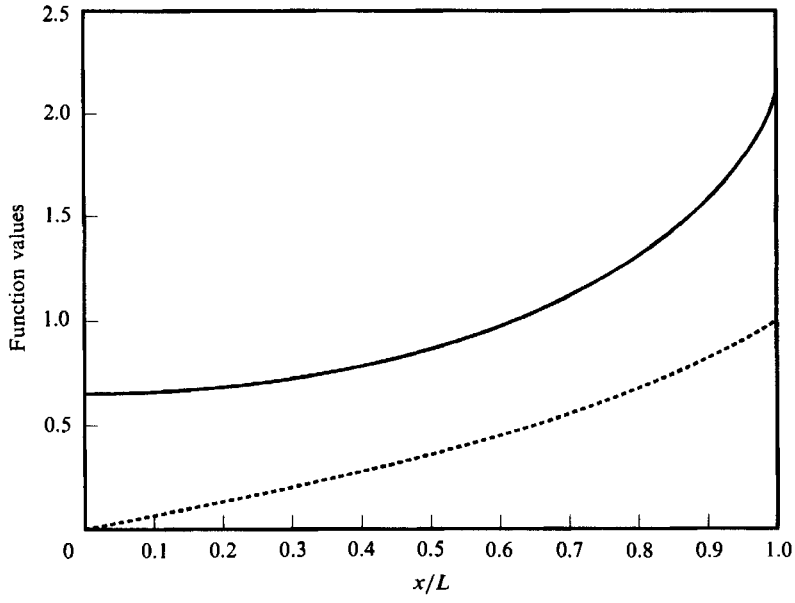

FIGURE 2. The functions $G(x/L)$ (----) and $G'(x/L)$ (——) for the sample case ($F(1) = 1.43$).

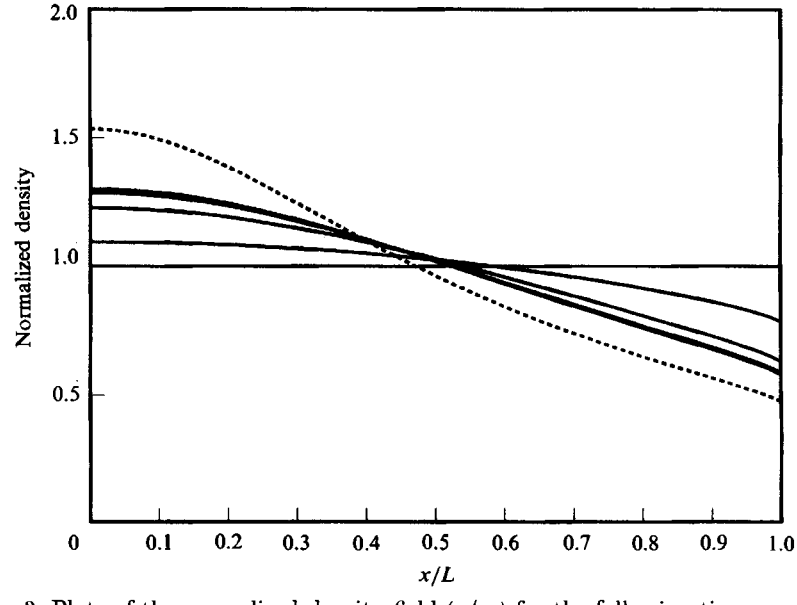

FIGURE 3. Plots of the normalized density field (ρ/ρ_0) for the following times: $-\infty$, -0.5 ms, 0 ms, 0.5 ms, ∞. The limiting normalized density field is shown as a dashed curve.

5.4. *Comparison of the theory and numerical simulations*

It is instructive to compare the analytical solution summarized above with a full gasdynamic numerical simulation of a one-dimensional problem. As an example, fission-fragment heating of argon ($\gamma = \frac{5}{3}$), initially at 101.3 kPa and 300 K, is considered. The gas is contained between two parallel walls that are 2 cm apart. On the inner surfaces of these walls are U_3O_8 foils that are 3 μm thick. These foils contain

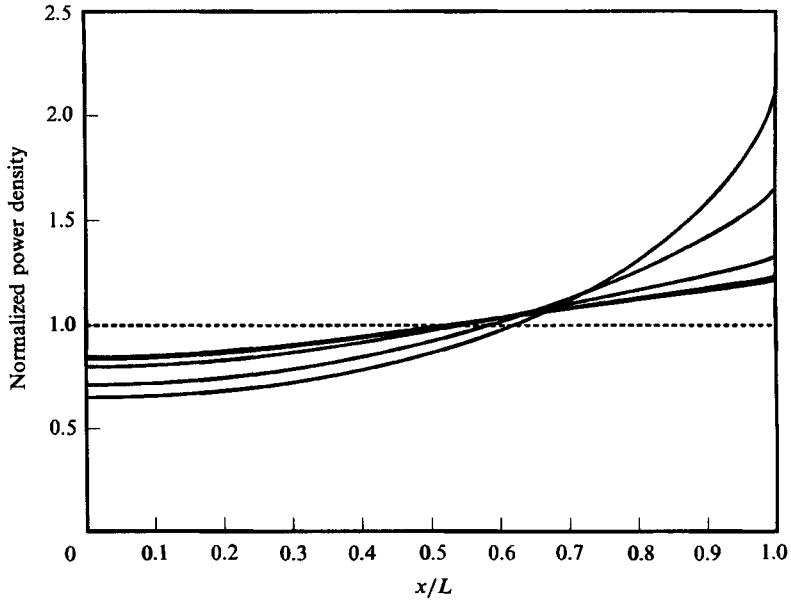

FIGURE 4. Plots of the normalized power density field $(Q/\bar{Q})$ for the following times: $-\infty$, -0.5 ms, 0 ms, 0.5 ms, ∞. The limiting normalized power density field is shown as a dashed curve.

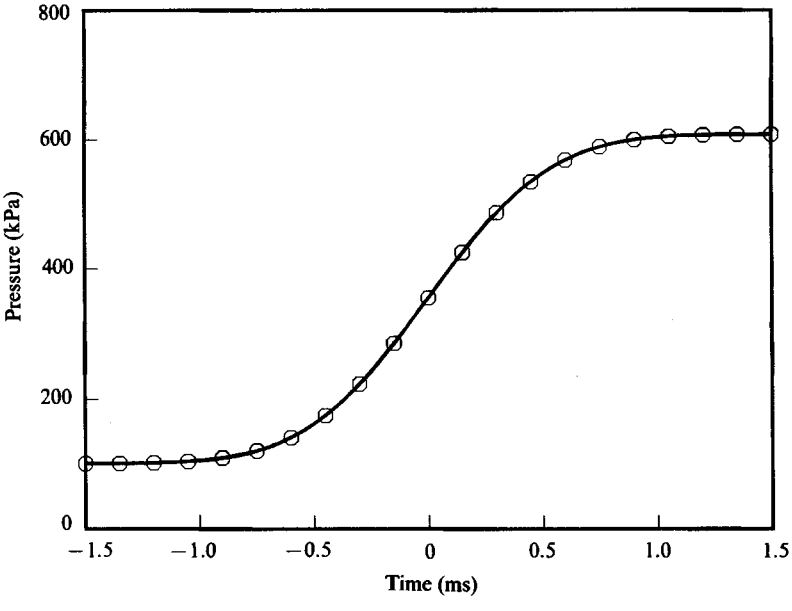

FIGURE 5. A comparison of the approximate analytical solution (——) and a numerical simulation (○): time variation of the mean pressure.

^{235}U atoms which undergo fission reactions when subjected to a flux of thermal neutrons. The power density scale of the pumping is chosen to be $Q_0 = 0.5$ kW/ml, and the function h is taken to be the Gaussian function

$$h(t/t_0) = \exp(-(t/t_0)^2) \tag{5.24}$$

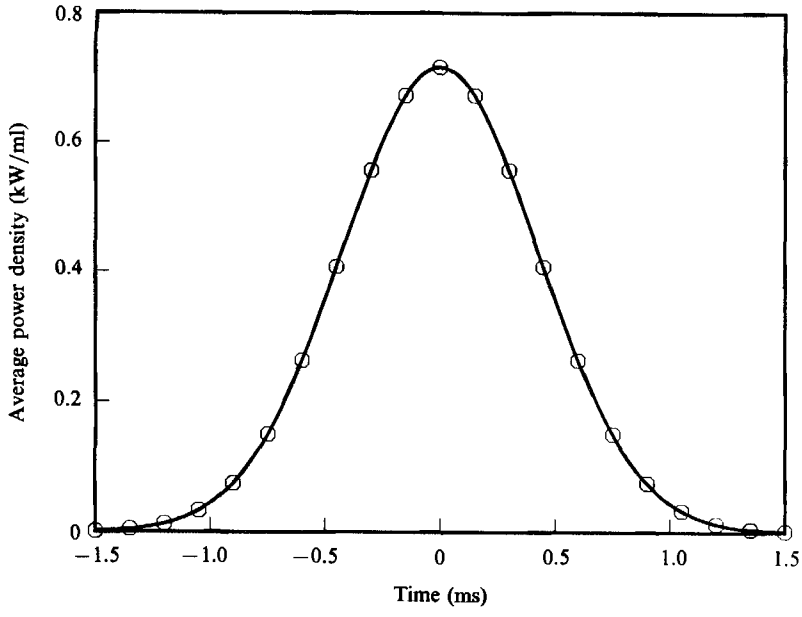

FIGURE 6. A comparison of the approximate analytical solution (——) and a numerical simulation (○): time variation of the average power density.

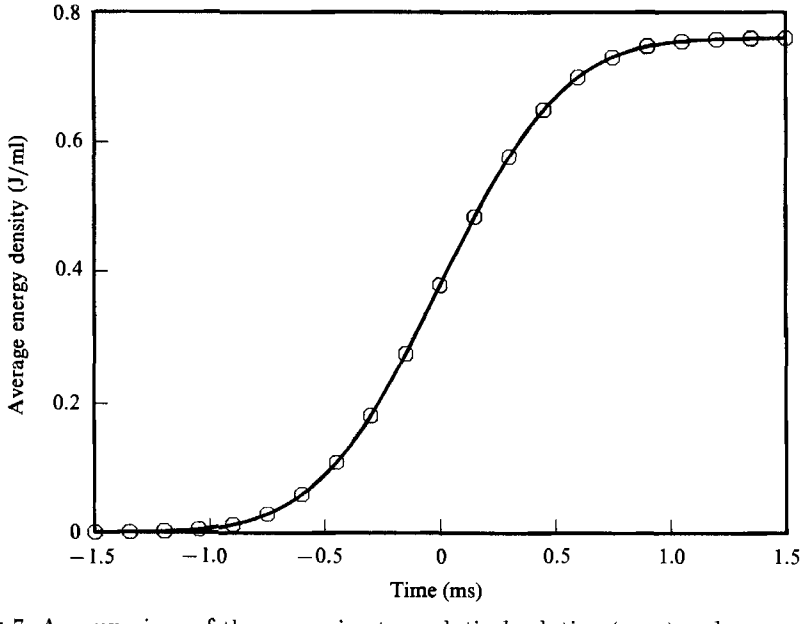

FIGURE 7. A comparison of the approximate analytical solution (——) and a numerical simulation (○): time variation of the average deposited energy density.

with $t_0 = 0.6$ ms. Note that h can be analytically integrated to yield

$$H(t/t_0) = \tfrac{1}{2}\pi^{\frac{1}{2}}(1 + \mathrm{erf}(t/t_0)). \tag{5.25}$$

The functions F and G are taken from the explicit representations for fission-fragment energy deposition given in Appendix A ($F(1) = 1.43$, and G and G' are

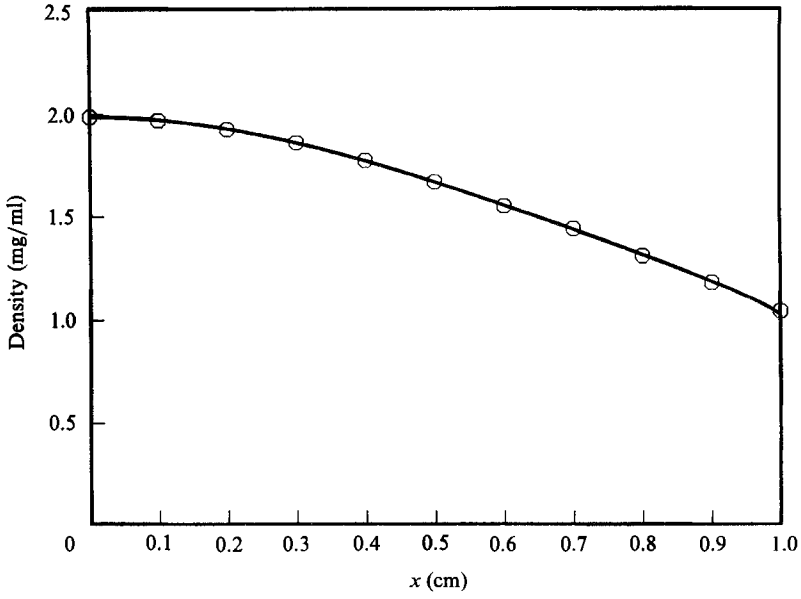

FIGURE 8. A comparison of the approximate analytical solution (——) and a numerical simulation (○): the density field at $t = 0$ (peak pumping).

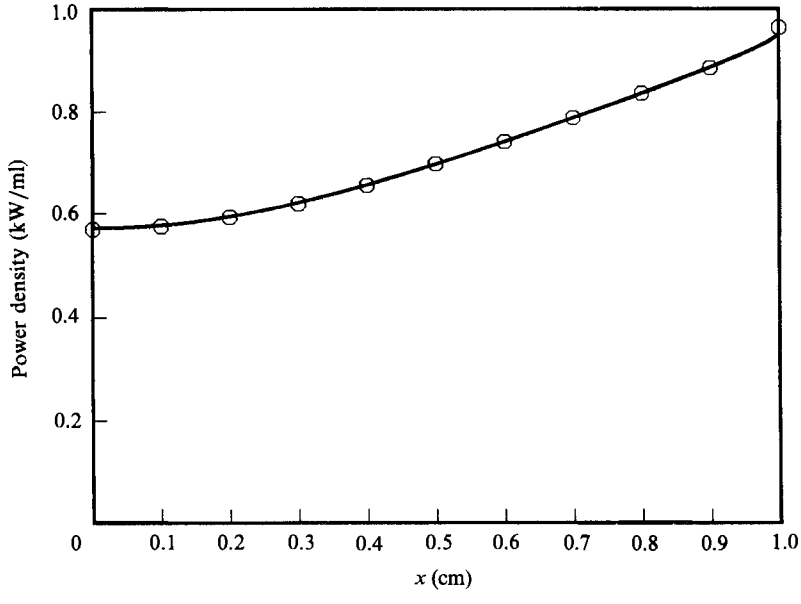

FIGURE 9. A comparison of the approximate analytical solution (——) and a numerical simulation (○): the power density field at $t = 0$ (peak pumping).

shown in figure 2). A check of the constraint shows that the theory is applicable to this case since $L/c_0 t_0 = 0.05 \ll 1$ ($c_0 = 323$ m/s). Moreover, $U_B/c_0 = 0.087$ and $\xi_m - G(\xi_m) = 0.15$, so (5.20) is satisfied as well.

Figures 3 and 4 show plots of normalized density (ρ/ρ_0) and normalized power density ($Q/\bar{Q}$) at a variety of different times ($-\infty$, -0.5 ms, 0 ms, 0.5 ms, ∞). The limiting profiles are also included for reference. Note that the limiting profiles are not

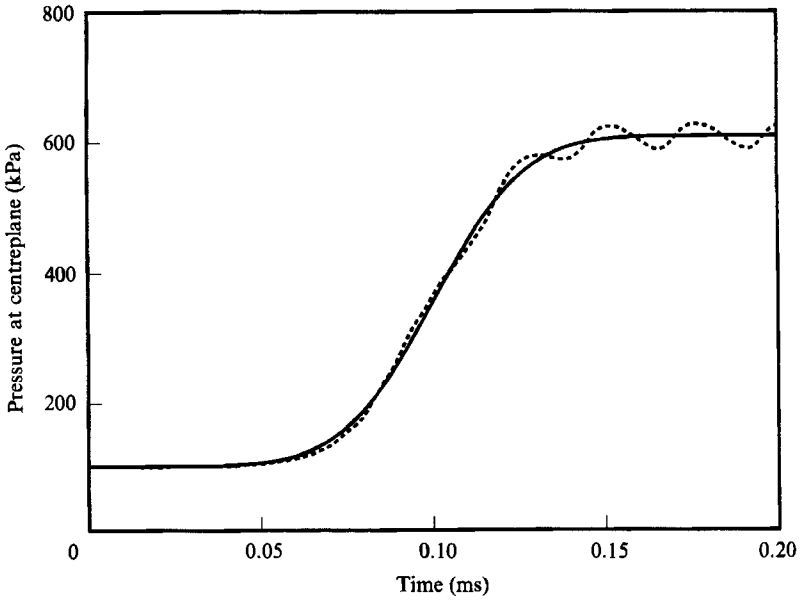

FIGURE 10. A comparison of the approximate analytical solution (——) and a numerical simulation (----) for a case in which $L/c_0 t_0 = 1$: the pressure at the centreplane as a function of time.

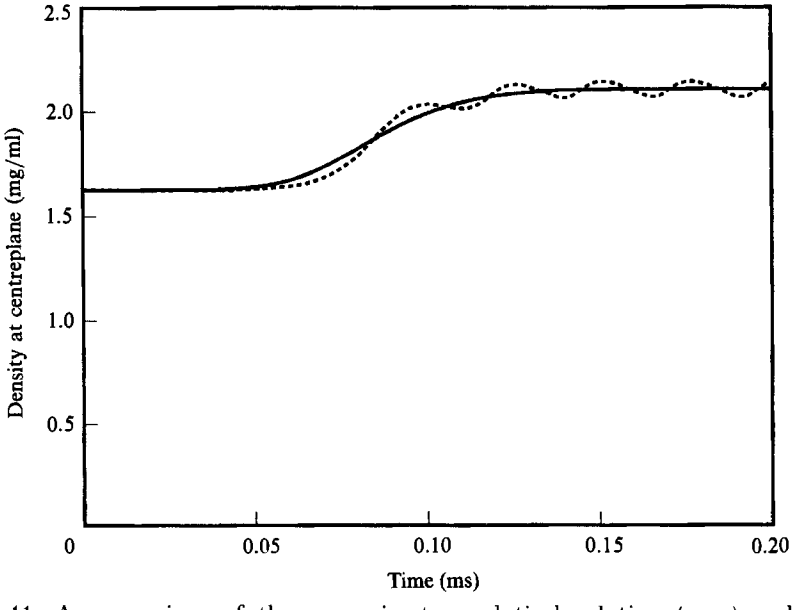

FIGURE 11. A comparison of the approximate analytical solution (——) and a numerical simulation (----) for a case in which $L/c_0 t_0 = 1$: the density at the centreplane as a function of time.

closely approached by the final ($t = \infty$) profiles. This is a consequence of the fact that in this case $(\bar{p}(\infty)/p_0)^{1/\gamma} \approx 3$, which is not much greater than unity.

Figures 5–9 show the pressure, average power density, the average net energy density, the density field at $t = 0$, and the power density field at $t = 0$ as calculated by the above analytical approach and by a state-of-the-art numerical simulation of the full gasdynamic problem. The agreement is excellent.

To demonstrate what happens as $L/c_0 t_0$ approaches unity, a case was studied which was identical to that above except that $t_0 = 0.03$ ms and $Q_0 = 10$ kW/ml. These values were chosen to satisfy $L/c_0 t_0 = 1$ while keeping the product $Q_0 t_0$ the same as in the above case. In other words, the same amount of energy was deposited, but the deposition was twenty times as fast. Figures 10 and 11 show the pressure and density at the centreplane as functions of time. The full gasdynamic simulation is observed to match the analytical solution of the acoustically filtered equations remarkably well in a time-averaged sense. However, the presence of 'ripples' in the full gasdynamic simulation is an indication of the fact that the acoustic-filtering assumptions are severely strained. If the time constant t_0 were reduced further while fixing the product $Q_0 t_0$, the amplitude of the ripples would be increased, and the situation would be more accurately described by the wave motion resulting from almost instantaneous deposition of energy, rather than by the acoustically filtered equations of motion.

6. Conclusions

Acoustic-filtering ideas have been applied to the equations describing the motion of a perfect gas in a closed geometry experiencing range-dependent volumetric heating. For the one-dimensional case, the acoustically filtered equations were solved analytically when written in Lagrangian form. This was due to the special form of the range-dependent volumetric heating source term. A constraint on the applicability of this approximate analytical solution was found by considering the underlying physical basis of the acoustic filtering ideas. Numerical simulation of cases satisfying this constraint produced results in excellent agreement with the theory.

The author wishes to thank R. J. Gross of Sandia National Laboratories for performing some of the numerical simulations included in this paper. This work was performed at Sandia National Laboratories, supported by the US DOE under contract number DE-AC04-76DP00789.

Appendix A. Calculation of the volumetric heating caused by fission fragments

The inner surface S of the volume V which contains the gas is coated with a foil, a thin layer of material containing fissionable atoms. When thermal neutrons encounter these atoms, fission reactions occur. The reaction products generally include several neutrons and two fission fragments, $\mathrm{FF}^{(1)}$ and $\mathrm{FF}^{(2)}$, which carry away as kinetic energy the bulk of the energy release during fission. Some of the fission fragments escape from the foils into the gas and there deposit a portion of their energy, where it is rapidly thermalized. There are also fission-fragment mass and momentum source terms in the gas, but they are completely negligible.

It is assumed that the fission fragments follow straight-line trajectories after creation, that the origins of the trajectories are distributed uniformly throughout the foil volume, and that the trajectories are isotropically distributed in solid angle (Miley & Thiess 1969). The following relation describes the energy of a fission fragment as it travels along its trajectory (Miley & Thiess 1969).

$$E^{(m)}(s_{\mathrm{f}}, s_{\mathrm{g}}) = E_0^{(m)}\left(1 - \frac{s_{\mathrm{f}}}{l_1^{(m)}} - \frac{1}{l_{2,0}^{(m)}}\int_{s_{\mathrm{f}}}^{s_{\mathrm{g}}} \frac{\rho(t, \boldsymbol{x}(s))}{\rho_0}\,\mathrm{d}s\right)^n. \tag{A 1}$$

Here, s_f is the distance $\mathrm{FF}^{(m)}$ travels from its origin within the foil to the foil surface, s_g is the distance it travels from its origin within the foil to the observation point within the gas, and s is the local coordinate along the trajectory with $s = 0$ corresponding to the trajectory origin. Thus, s_f, s_g, and $\boldsymbol{x}(s)$ depend on the origin and angular orientation of the trajectory. The quantities $E_0^{(m)}$, $l_1^{(m)}$, and $l_{2,0}^{(m)}$ are the initial energy, the range in the foil material, and the range in the gas (when the density is uniformly ρ_0), respectively, of the $\mathrm{FF}^{(m)}$.

Consider a small volume ΔV of gas within the chamber. In order to calculate the volumetric heating source term, the energy ΔE deposited in ΔV by all fission fragments passing through ΔV in a small amount of time Δt must be summed. Thus, a multiple integration must be performed which consists of a triple integral over all possible trajectory origins (uniformly distributed within the foil volume) and a double integral over all possible trajectory directions (isotropically distributed in solid angle). If a trajectory misses ΔV, it will obviously contribute no energy. If a trajectory intersects ΔV, the energy it deposits in ΔV will be the energy it loses in ΔV based on (A 1). Finally, the limit $\Delta V \to 0$ must be taken to find Q, which is defined as

$$Q \equiv \lim_{\Delta V \to 0} \left(\frac{\Delta E}{\Delta t \Delta V} \right). \tag{A 2}$$

Taking this limit in effect undoes the double integral over solid angle. Moreover, one integral of the remaining triple integral over the foil volume can be performed analytically using the explicit representation of the fission-fragment energy given in (A 1).

The final result for an arbitrary volume V filled with a gas of an arbitrary density distribution $\rho(t, \boldsymbol{x})$ and mean density ρ_0 is expressed as

$$\begin{aligned} Q(t, \boldsymbol{x}) = {} & \frac{\Phi(t/t_0)\, \sigma \nu E_{\mathrm{ref}}}{4\pi} \frac{\rho(t, \boldsymbol{x})}{\rho_0} \sum_{m=1}^{2} \frac{E_0^{(m)}}{E_{\mathrm{ref}}} \frac{l_1^{(m)}}{l_2^{(m)}} \\ & \times \int_{4\pi} \left[\left(\max\left\{ 0, \left(1 - \frac{1}{l_2^{(m)}} \int_0^{r_1(\Omega)} \frac{\rho(t, r(\Omega))}{\rho_0} \mathrm{d}r \right) \right\} \right)^n \right. \\ & \left. - \left(\max\left\{ 0, \left(1 - \frac{1}{l_2^{(m)}} \int_0^{r_1(\Omega)} \frac{\rho(t, r(\Omega))}{\rho_0} \mathrm{d}r - \frac{r_2(\Omega) - r_1(\Omega)}{l_1^{(m)}} \right) \right\} \right)^n \right] \mathrm{d}\Omega. \end{aligned} \tag{A 3}$$

In the prefactor, Φ is the time-varying, spatially uniform neutron flux, σ is the cross-section (area) for the fission reaction, ν is the number density of fissionable atoms in the foil, and E_{ref} is an arbitrary reference energy. These quantities are related to the quantities Q_0 and $h(t/t_0)$ by

$$Q_0 h(t/t_0) \equiv \Phi(t/t_0)\, \sigma \nu E_{\mathrm{ref}}. \tag{A 4}$$

The quantity $r(\Omega)$ refers to distances measured from the observation point in the gas along the trajectory, and the quantities $r_1(\Omega)$ and $r_2(\Omega)$ are the distances to the inner and outer surfaces of the foil, respectively. The solid angle Ω and the distance r are thus a polar coordinate system with origin located at the observation point in the gas.

For the one-dimensional geometry considered in this paper, when the inner surfaces of both walls are coated with foils of uniform thickness W, these integrals can be performed analytically if the gas density is uniform (Miley & Thiess 1969). Since the density only enters the solution in the *argument* of the function and does not affect the *form*, these results can be taken over directly to the case of non-uniform

density. Below is a summary of the specific form of the equations for F and F' describing the fission-fragment volumetric heating source term $f[x;1]$:

$$G(\xi) = F(\xi)/F(1), \tag{A 5}$$

$$F'(\xi) = \sum_{m=1}^{2} \frac{E_0^{(m)}}{E_{\text{ref}}} \frac{l_1^{(m)}}{l_{2,0}^{(m)}} [I_n(p_+^{(m)}(\xi)) + I_n(p_-^{(m)}(\xi)) - I_n(q_+^{(m)}(\xi)) - I_n(q_-^{(m)}(\xi))], \tag{A 6}$$

$$F(\xi) = \sum_{m=1}^{2} \frac{E_0^{(m)}}{E_{\text{ref}}} \frac{l_1^{(m)}}{L} [J_n(p_+^{(m)}(\xi)) - J_n(p_-^{(m)}(\xi)) - J_n(q_+^{(m)}(\xi)) + J_n(q_-^{(m)}(\xi))], \tag{A 7}$$

$$I_n(z) = \frac{n}{2} \sum_{k=1}^{\infty} \frac{\max(z,0)^{n+k}}{(n+k)(n+k-1)}, \tag{A 8}$$

$$J_n(z) = \frac{n}{2} \sum_{k=1}^{\infty} \frac{\max(z,0)^{n+k+1}}{(n+k+1)(n+k)(n+k-1)}, \tag{A 9}$$

$$p_+^{(m)}(\xi) = 1 - (L/l_{2,0}^{(m)})(1-\xi), \tag{A 10}$$

$$p_-^{(m)}(\xi) = 1 - (L/l_{2,0}^{(m)})(1+\xi), \tag{A 11}$$

$$q_+^{(m)}(\xi) = p_+^{(m)}(\xi) - W/l_1^{(m)}, \tag{A 12}$$

$$q_-^{(m)}(\xi) = p_-^{(m)}(\xi) - W/l_1^{(m)}, \tag{A 13}$$

The $p_+^{(m)}$ and $q_+^{(m)}$ terms are contributions from the foil located at $x = +L$, and the $p_-^{(m)}$ and $q_-^{(m)}$ terms are contributions from the foil located at $x = -L$.

Table 1 contains the relevant parameters (Chung & Prelas 1984) for the fission reaction involving ^{235}U atoms in U_3O_8 foils:

$$^{235}_{92}\text{U} + {}^{1}_{0}\text{n}_{\text{thermal}} \rightarrow \{\text{several}\}{}^{1}_{0}\text{n} + \text{FF}^{(1)} + \text{FF}^{(2)}. \tag{A 14}$$

Gas densities correspond to values at $p_{\text{ref}} = 101.3$ kPa and $T_{\text{ref}} = 288$ K. Ranges in gases are inversely proportional to the density.

$$l_{2,0}^{(m)} = l_{2,\text{ref}}^{(m)} \left(\frac{p_{\text{ref}}}{p_0} \frac{T_0}{T_{\text{ref}}} \right). \tag{A 15}$$

Parameters for other fission reactions can be found in Kahn, Harman & Forgue (1965), Nguyen & Grossman (1967), Miley & Thiess (1969), Miley (1970), and Guyot, Miley & Verdeyen (1972). Chung & Prelas (1984) also give calculations for cylindrical geometries.

Appendix B. The acoustic-filtering methodology (Paolucci 1982)

Full implementation of acoustic filtering generates a hierarchy of equations, which result from the consistent expansion of the problem variables in terms of a small parameter. This small parameter is the Mach-number scale M. The following expansions are used:

$$p = p^{(0)} + M^2 p^{(1)} + \ldots, \tag{B 1}$$

$$\rho = \rho^{(0)} + M^2 \rho^{(1)} + \ldots, \tag{B 2}$$

$$T = T^{(0)} + M^2 T^{(1)} + \ldots, \tag{B 3}$$

$$\boldsymbol{u} = M(\boldsymbol{u}^{(0)} + M^2 \boldsymbol{u}^{(1)} + \ldots). \tag{B 4}$$

Parameter	Value
n	1.45
$E_0^{(1)}$	67.5 MeV
$E_0^{(2)}$	98.7 MeV
E_{ref}	0.01 MeV
$l_1^{(1)}$ in U_3O_8	10.4 μm
$l_1^{(2)}$ in U_3O_8	13.5 μm
$l_{2,\mathrm{ref}}^{(1)}$ in Argon	1.94 cm
$l_{2,\mathrm{ref}}^{(2)}$ in Argon	2.39 cm

TABLE 1. Fission-fragment energy deposition model parameters

The source term Q, which sets the velocity scale, must also be expanded:

$$Q = M(Q^{(0)} + M^2 Q^{(1)} + \ldots). \tag{B 5}$$

Since attention is focused on the timescale commensurate with the particle velocity rather than the speed of sound, the time variable is also rescaled:

$$\bar{t} = Mt. \tag{B 6}$$

Insertion of these expansions into the conservation equations and elimination of the higher-order terms yields the following equations:

$$\frac{\partial}{\partial \bar{t}} \rho^{(0)} + \nabla \cdot \rho^{(0)} \boldsymbol{u}^{(0)} = 0, \tag{B 7}$$

$$\nabla p^{(0)} = 0, \tag{B 8}$$

$$\frac{\partial}{\partial \bar{t}} p^{(0)} + \gamma p^{(0)} \nabla \cdot \boldsymbol{u}^{(0)} + \boldsymbol{u}^{(0)} \cdot \nabla p^{(0)} = (\gamma - 1) Q^{(0)}, \tag{B 9}$$

$$p^{(0)} = R\rho^{(0)} T^{(0)} = (\gamma - 1) \rho^{(0)} e^{(0)}, \tag{B 10}$$

$$\nabla p^{(1)} = -\rho^{(0)} \frac{\mathrm{D}^{(0)}}{\mathrm{D}\bar{t}} \boldsymbol{u}^{(0)}. \tag{B 11}$$

When $p^{(0)}$, $\rho^{(0)}$, $T^{(0)}$, $M\boldsymbol{u}^{(0)}$, $MQ^{(0)}$, and $M^2 p^{(1)}$ are identified with $\bar{p}$, ρ, T, $\boldsymbol{u}$, Q, and $\hat{p}$, respectively, these equations are seen to be the equations of §2. The pressure variation $\hat{p}$ is also constrained to have zero mean,

$$\frac{1}{V} \int_V \hat{p}(t, \boldsymbol{x}) \, \mathrm{d}^3 \boldsymbol{x} = 0. \tag{B 12}$$

It is possible to solve the one-dimensional versions of (B 11) and (B 12) using the results of §4. Here, $\hat{p}_{\mathrm{p}}$ is the pressure perturbation following the Lagrangian particles:

$$\frac{\hat{p}_{\mathrm{p}}}{p_0} = \left\{ -\frac{\rho_0 L^2}{p_0} \frac{\mathrm{d}^2}{\mathrm{d}t^2} \left(\frac{\bar{p}}{p_0} \right)^{-1/\gamma} \right\} \left\{ \int_0^{x_0/L} (\xi - G(\xi)) \, \mathrm{d}\xi \right.$$
$$\left. - \int_0^1 (1 - \xi)(\xi - G(\xi)) \, \mathrm{d}\xi - (1 - (\bar{p}/p_0)^{-1/\gamma}) \int_0^1 (\xi - G(\xi))^2 \mathrm{d}\xi \right\}. \tag{B 13}$$

Note that the last two integrals are positive numbers and the first integral is a

function that need be tabulated only once. Typically, the quantity contained in the first set of braces is positive for early times in the pulse and negative for later times. The quantity contained in the second set of braces is negative for $x_0 = 0$, positive for $x_0 = L$, and increases monotonically in between. Thus, early in the pulse, the pressure gradients act to accelerate the flow inward, whereas at later times the pressure gradients act to decelerate the established inward flow, bringing it eventually to rest (the *flow* is always inward). Note in passing that, in accord with the expansion,

$$\frac{\hat{p}_p}{p_0} = O\left(\frac{\rho_0 L^2}{p_0 t_0^2}\right) = O\left[\left(\frac{L/t_0}{c_0}\right)^2\right] = O(M^2). \tag{B 14}$$

Appendix C. Flow in an infinite, unbounded volume

As in earlier sections, the energy deposition Q, with scale Q_0, is taken to release a finite amount of energy over a timescale t_0 in a finite central region characterized by a lengthscale L, where $L/c_0 t_0 \ll 1$.

Relations analogous to those of §2 are obtained by formally allowing V to become infinite. In this limit, $\bar{Q}$ vanishes identically, and hence $\bar{p}$ is a constant with value p_0. Equations (2.1), (2.11), and (2.9) become the following:

$$\frac{\partial}{\partial t}\rho + \nabla\cdot\rho\boldsymbol{u} = 0, \tag{C 1}$$

$$\frac{\partial}{\partial t}\rho\boldsymbol{u} + \nabla\cdot\rho\boldsymbol{u}\boldsymbol{u} = -\nabla\hat{p}, \tag{C 2}$$

$$\gamma p_0 \nabla\cdot\boldsymbol{u} = (\gamma-1)\,Q(t,\boldsymbol{x}). \tag{C 3}$$

From (C 3), the maximum velocity is seen to scale with $Q_0 L/p_0$. In order to fulfill the condition that Mach numbers be small, the relation $Q_0 L/p_0 c_0 \ll 1$ must be satisfied.

Outside the central region, Q vanishes identically. Therefore, $\boldsymbol{u}$ is divergence-free, so (C 1)–(C 3) reduce to the equations for incompressible flow. Thus, the far-field flow predicted by formal application of the theory is incompressible flow driven by an expanding region.

Two remarks can be made about this observation. First, if one is concerned with precise qualitative and quantitative details of the far-field wave propagation produced by the central expanding region, this methodology does not provide a satisfactory result (by definition, it was not expected to) since in reality there is a front propagating outward with speed c_0 ahead of which there is no disturbance. Second, if one is concerned with flow details on the scales of the perturbations produced in the central region, then it is conjectured that this methodology gives a reasonable approximation to the flow field at a point for times much larger than the maximum of t_0 and the time required for acoustic signals from the central region to reach the point.

REFERENCES

BAUM, H. R., REHM, R. G., BARNETT, P. D. & CORLEY, D. M. 1983 Finite difference calculations of buoyant convection in an enclosure, I. the basic algorithm. *SIAM J. Sci. Stat. Comput.* **4**, 117–135.

BORN, M. & WOLF, E. 1980 *Principles of Optics*. Pergamon.

CHUNG, A. K. & PRELAS, M. A. 1984 The transport of heavy charged particles in a cylindrical nuclear-pumped plasma. *Nucl. Sci. Engng* **86**, 267–274.

GUYOT, J. C., MILEY, G. H. & VERDEYEN, J. T. 1972 Application of a two-region heavy charged particle model to noble-gas plasma induced by nuclear radiation. *Nucl. Sci. Engng* **48**, 373–386.

KAHN, S., HARMAN, R. & FORGUE, V. 1965 Energy distributions of fission fragments from uranium dioxide films. *Nucl. Sci. Engng* **23**, 8–20.

MCARTHUR, D. A. & TOLLEFSRUD, P. B. 1975 Observation of laser action in CO gas excited only by fission fragments. *Appl. Phys. Lett.* **26**, 187–190.

MILEY, G. H. 1970 *Direction Conversion of Nuclear Radiation Energy.* American Nuclear Society.

MILEY, G. H. & THIESS, P. E. 1969 A unified approach to two-region ionization-excitation density calculations. *Nucl. Appl.* **6**, 434–451.

NEAL, D. R., SWEATT, W. C., TORCZYNSKI, J. R., GROSS, R. J., ALFORD, W. J., MCARTHUR, D. A. & HAYS, G. N. 1987 Time-resolved phase-front measurements of a pulsed laser gain region. Presented at the *17th Winter Colloquium on Quantum Electronics, Snowbird, Utah.*

NGUYEN, D. H. & GROSSMAN, L. M. 1967 Ionization by fission fragments escaping from a source medium. *Nucl. Sci. Engng* **30**, 233–241.

PAOLUCCI, S. 1982 On the filtering of sound from the Navier–Stokes equations. *Sandia Rep.* SAND82-8257. Sandia National Laboratories.

PLASS, G. N. & YATES, H. 1965 Atmospheric phenomena. In *Handbook of Military Infrared Technology* (ed. W. L. Wolfe), Chap. 6. Office of Naval Research.

REHM, R. G. & BAUM, H. R. 1978 The equations of motion for thermally driven, buoyant flows. *Natl Bur. Stand. J. Res.* **83**, 297–308.

SAMLIN, G. E. & PATTERSON, E. L. 1987 A 1-ms electron beam facility for laser kinetics studies. *Proc. the Ninth International Conference on Lasers and Applications (Lasers '86).* STS Press.

SCHUTT, J. A. & BAER, M. R. 1987 Numerical simulation of buoyant convection in vented enclosures. *Sandia Rep.* SAND86-0790. Sandia National Laboratories.

TORCZYNSKI, J. R. & GROSS, R. J. 1986 Response of gases to large, transient, nonuniform heating from external radiation sources. *Bull. Am. Phys. Soc.* **31**, 1738.